Influence of preparation procedure on catalytic activity of PdBEA zeolites in aqueous phase hydrodechlorination of 1,1,2-trichloroethene

Izabela I. Kamińska, Dmytro Lisovytskiy, Sandra Casale, Anna Śrębowata, Stanislaw Dzwigaj

Influence of preparation procedure on catalytic activity of PdBEA zeolites in aqueous phase hydrodechlorination of 1,1,2-trichloroethene

Izabela I. Kamińska[a,*], Dmytro Lisovytskiy[a], Sandra Casale[b], Anna Śrębowata[a], Stanislaw Dzwigaj[b,*]

[a]Institute of Physical Chemistry, PAS, Kasprzaka 44/52, PL-01224 Warsaw, Poland

[b]Sorbonne Universités, UPMC Univ Paris 06, CNRS, UMR 7197, Laboratoire de Réactivité de Surface, 4 place Jussieu, Case 178, 75252 Paris, France

Figures: 10

Tables: 3

Keywords: Pd, BEA, 1,1,2-trichloroethene, aqueous-phase hydrodechlorination

*Corresponding authors:

Izabela I. Kamińska, e-mail: iikaminska@ichf.edu.pl, tel.: +48 1 22 343 3360

Stanislaw Dzwigaj, e-mail: stanislaw.dzwigaj@upmc.fr, tel.: +33 1 44 27 21 13

Abstract

Pd-loaded BEA zeolites containing 1 wt % of Pd were prepared by a two-step postsynthesis method (PdSiBEA and PdSiAlBEA) and a conventional wet impregnation (PdHAlBEA). Modification of BEA zeolite resulted in the introduction of Pd ions into zeolite framework as pseudo-tetrahedral Pd(II) and extra-framework octahedral Pd(II) evidenced by XRD, DR UV–vis and TPR measurements. Calcination of as prepared zeolites in air at 773 K for 3 h and then reduction in 10 % H_2/Ar flow at 873 K for 3 h led to obtain red-C-PdSiBEA, red-C-PdSiAlBEA and red-C-PdHAlBEA zeolites with different Pd nanoparticles size distributions showed by TEM. These zeolite materials were found to be active catalysts in aqueous-phase hydrodechlorination of 1,1,2-trichloroethene (TCE). The conducted catalytic reactions have demonstrated that the rate and course of TCE hydrodechlorination depend on the catalysts preparation method and Pd nanoparticles size.

1. Introduction

Palladium as noble metal has a wide application in catalytic reactions. It accelerates many hydrogenation and dehydrogenation reactions due to its excellent properties [1-4]. Palladium is also the most extensively used metal in purification of air and water containing toxic substances such as volatile organic compounds (VOCs) [5, 6]. Particular attention should be focused on the removal of chlorinated hydrocarbons like 1,2-dichloroethane (DCA), 1,1,2-trichloroethene (TCE) and 1,1,2,2-tetrachloroethene (PCE), because of their potential carcinogenic and mutagenic effects on living organisms [7-9]. The application of Pd in the hydrodechlorination (HDC) processes allows to easily, cheaply and without damage of environment transforming harmful chemicals into less toxic products like ethane or ethene [10-12].

High hydrodechlorination efficiency of Pd could be affected by a number of factors such as the metallic nanoparticle size, its shape, oxidation state and interaction with the support, among others [13, 14]. A number of authors have deduced that Pd nanoparticle size is crucial for the performance of HDC reactions [15-20]. One of their hypothesis is that bigger Pd nanoparticles are more active and resistant for reaction conditions [15-17]. However, the others have proved the superiority of small nanoparticles, because of its higher surface-to-volume ratio [18-20]. One of the first reports pertains to research carried out by Juszczyk et al. [15]. They noticed that catalytic activity of $Pd/\gamma\text{-}Al_2O_3$ in gas-phase hydrodechlorination of CCl_2F_2 was strongly related to Pd dispersion: the samples with the lowest metal dispersion exhibited the highest turnover frequencies. Aramendía et al. [16] observed similar effect in liquid-phase hydrodechlorination of chlorobenzene over Pd-supported catalysts. In this case, the change of dispersion from 54 to 7 % corresponded to an increase in catalytic activity by a factor of 20. In addition, they noticed a better resistance to chlorine, when the size of Pd nanoparticles increased.

On the other hand, several authors present a different view [18-20]. Gómez-Quero et al. [18] analyzed the effect of metal dispersion on the liquid-phase hydrodechlorination of 2,4-dichlorophenol over Pd/Al_2O_3. They observed a significant decrease in reaction rate with a decrease in palladium dispersion from 67 % to 25 %, with only residual activity in case of the catalyst with 8 % dispersion. Dong et al. [19] also reported that magnetic porous carbon composite supported palladium nanoparticles (5 nm) displayed high efficiency in HDC of chlorophenols.

Moreover, the appropriate support has also a significant influence on catalytic activity and stability of Pd catalysts [17]. The most popular Pd supports are activated carbons, silica, titania and alumina [15-19, 21]. Recently, the significant surge of interest in zeolite materials has been observed due to their specific properties (cation exchange, shape selectivity and acidity) [20,22,23]. Śrębowata et al. [20] have found a beneficial effect of desilication of HZSM-5 zeolite on PdHZSM-5 activity in aqueous-phase hydrodechlorination of TCE. It seems to us to be very interesting to investigate the influence of dealumination process on the activity of Pd-loaded zeolites in TCE removal from water. Therefore, we decided to synthetize Pd-loaded BEA zeolites with different dealumination stage and checked their properties by characterization using different techniques and investigated catalytic reaction with TCE in aqueous-phase.

Very interesting results obtained for transition metals-loaded BEA zeolites used in gas-phase HDC [24-27] were the motivation to investigate the effect of preparation procedure on the catalytic properties of Pd-loaded BEA zeolites in aqueous phase hydrodechlorination of 1,1,2-trichloroethene.

2. Experimental

2.1. Catalysts preparation

TEABEA zeolite (Si/Al = 19) provided by RIPP (China) was divided into three portions. First portion was treated by a 13 mol L^{-1} HNO_3 solution for 4 h at 343 K to obtain completely dealuminated SiBEA zeolite (Si/Al = 1300). Second portion was treated by a 13 mol L^{-1} HNO_3 solution for 3.5 h at 343 K to obtain partially dealuminated SiAlBEA zeolite (Si/Al = 940). The resulting zeolites with vacant T-sites were recovered by centrifugation, washed with distilled water and dried overnight at 353 K. Third portion of TEABEA was calcined in air at 823 K for 15 h under static conditions to remove organic template, then treated two times with 0.1 mol L^{-1} NH_4NO_3 solution (400 mL) during 3 h at 343 K. Resulted NH_4AlBEA was washed with distilled water and dried overnight at 363 K and next calcined in air at 773 K for 3 h under static conditions to remove NH_3 and obtain HAlBEA zeolite (Si/Al = 17).

Palladium-loaded BEA zeolites were prepared by impregnation of SiBEA, SiAlBEA and HAlBEA under ambient conditions by a 9.4×10^{-4} mol dm^{-3} aqueous solution of $PdCl_2$ (pH in the range of 3.0 – 3.4). First, 2 g of each zeolite materials were stirred at room temperature for 24 h in excess solvent using 200 ml of the palladium chloride solution (pH in the range of 2.9 – 3.3) and then the suspensions were stirred in a rotary vacuum evaporator at 333 K for 2 h until complete evaporation of water. The resulting light-brown solids containing 1 wt % of Pd were labelled as PdSiBEA, PdSiAlBEA and PdHAlBEA. Next, all these materials were calcined in air flow at 773 K for 3 h and labeled C-PdSiBEA, C-PdSiAlBEA and C-PdHAlBEA, respectively. Then, small portions of these materials were reduced at 873 K for 3 h in 10 % H_2/Ar flow to obtain red-C-PdSiBEA, red-C-PdSiAlBEA and red-C-PdHAlBEA.

2.2. Catalysts characterization and catalytic tests

2.2.1. Diffuse Reflectance UV-vis Spectroscopy

Diffuse Reflectance (DR) UV-vis spectra of as prepared samples were recorded at ambient atmosphere on a Cary 5000 Varian spectrometer (DR UV–Vis scan rate 10 nm s^{-1}, data interval 1 nm) equipped with a double integrator with polytetrafluoroethylene as reference.

2.2.2. Physisorption

Surface areas and porosities of calcined samples were measured with an ASAP 2020 instrument from Micromeritics, employing the BET (Brunauer-Emmett-Teller) and HK (Horwath-Kawazoe) methods using nitrogen as adsorbate. Before measuring the adsorption isotherm at 77 K, the samples were kept at 473 K for 4 h in vacuum remove adsorbed water and gases.

2.2.3. Temperature-Programmed Reduction

Temperature-Programmed Reduction (TPR) of calcined samples was carried out using glass flow system equipped with a Gow-Mac thermal conductivity detector. TPR runs were performed in 10% H_2/Ar flow (25 cm^3 min^{-1}), ramping the temperature at 10 K min^{-1}, started from 260 K to 973 K. Injections of known amounts of hydrogen into the H_2/Ar flow were provided for calibration (before and after each TPR run).

2.2.4. Chemisorption

Chemisorption measurements of CO using a conventional static method were carried out with an ASAP 2020 Chem. instrument from Micromeritics. Prior to chemisorption measurement 0.1 g of calcined Pd-loaded BEA zeolite was reduced in 10 % H_2/Ar flow (25 cm^3 min^{-1}), ramping the temperature from room to 873 K (at 10 K min^{-1}) and kept at 873 K for 3 h. Then the catalysts were cooled down to the room temperature and connected with the ASAP 2020 Chem. instrument. Chemisorption measurements were carried out according to the procedure described previously [24].

2.2.5. TCE hydrodechlorination

Hydrodechlorination of TCE in aqueous-phase were performed in a 500 mL round bottomed flask equipped with a pH-meter, magnetic stirring bar and temperature controller, using 350 mL of MiliPore water and 20 µL of TCE and 0.1 g of reduced catalyst (at 873 K for 3 h in 10 % H_2/Ar flow). Each reaction was carried out at 303 K with continuous stirring (1000 rpm). Before adding the substrate, the water had been saturated with hydrogen for 30 min and then the catalyst was added to reaction mixture. Reaction samples were taken at 0, 2, 5, 10, 15, 20, 60, 90, 120 and 150 minutes of reaction. The substrate concentration and product distributions were monitored using a gas chromatographic set-up (Bruker 456-GC with ECD and FID detectors, Headspace SHS-40) at it was reported earlier [25]. Samples after hydrodechlorination of TCE were labelled as spent-red-C-PdSiBEA, spent-red-C-PdSiAlBEA and spent-red-C-PdHAlBEA, respectively.

2.2.6. X-Ray Diffraction

X-Ray Diffractograms (XRD) of as prepared samples were recorded at ambient atmosphere on a BRUKER D8 Advance diffractometer using the Cu Kα radiation (λ = 154.05 pm) in the 2θ range of 5 – 90°. XRD profiles of samples after reduction and reaction were recorded on a Siemens D5000 diffractometer using Ni-filtered Cu Kα radiation in the 2θ range of 5 – 90°.

2.2.7. Transmission Electron Microscopy

Transmission Electron Microscopy (TEM) studies for the catalysts after reduction step and after catalytic reaction were carried out using JEOL JEM-100CXII electron microscope operated at an acceleration voltage of 100 keV. The samples before TEM investigations were dispersed in pure alcohol using ultrasonic cleaner and putting a drop of this suspension on carbon films on copper grids.

3. Results and discussion

3.1. DR UV-vis studies

Fig. 1 shows DR UV-Vis spectra of as prepared samples. DR UV–Vis spectrum of HAlBEA contains two bands at 220 and 270 nm probably related to Al species present in zeolite structure, in line with earlier report [26]. Process of dealumination changes the position of these bands from 220 to 206 nm and from 270 to 282 nm for SiAlBEA; from 220 to 200 nm and from 270 to 297 nm for SiBEA. On the other hand, the palladium-loaded BEA zeolites exhibit two characteristic bands at about 264 – 288 and 390 nm. First band can be assigned to oxygen-to-metal charge transfer (CT) transitions involving pseudo-tetrahedral Pd(II), while second one, wide and less intense, can be assigned to extra-framework octahedral Pd(II) [28-31]. The presence of extra-framework Pd(II) is confirmed by the light brown color of the samples.

3.2. Physisorption studies

The nitrogen adsorption–desorption isotherms of calcined zeolites and catalysts (**Fig. 2**) look similar and can be classified as type I according to IUPAC. All zeolite materials are characterized by BET surface area in the range of 310 – 477 $m^2\ g^{-1}$ and pore volume in the range of 0.13 – 0.16 $cm^3\ g^{-1}$ (**Table 1**). These comparable results indicate that the textural properties of BEA zeolite are preserved upon methods of their preparation. Generally, as-prepared Beta zeolites have higher specific surface areas [32,33]. The decreasing of specific surface areas in C-SiBEA, C-SiAlBEA and C-HAlBEA in comparinon with as-prepared samples can be probably the effect of some blocking of the pore during the calcination. The incorporation of Pd^{2+} ions in as prepared Beta zeolites can stabilize the zeolite structure and prevent the blocking of pores during calcination, therefore there is more available space for nitrogen adsorption and in consequence higher surface areas, and micropores and mesopores volumes (**Table 1**).

3.3. H_2-TPR studies

H_2-TPR measurements were carried out to determine the differences in reducibility of palladium species present in C-PdSiBEA, C-PdSiAlBEA and C-PdHAlBEA zeolites. Each of TPR patterns contains three or four reduction peaks (**Fig. 3**). According to the literature [27,34], the peaks with the maxima at the lowest temperatures (260 – 273 K) are originated from the reduction of PdO species located in main channels of zeolite and/or weakly bounded to zeolite structure. It is well known that PdO can be reduced in easy way at very low temperatures (even about 273 K) on some supports [35]. The peaks with the maxima at higher temperatures (311 – 318 K) can be attributed to the reduction of octahedral Pd(II) present at extra-framework position, whereas the peaks at temperatures 347 – 382 K can be assigned to the reduction of mononuclear Pd(II) present in framework or exchange position, where the stabilization of Pd^{2+} ions is improved by higher negative charge density of the support [27, 34]. The negative H_2 consumption peak at 380 – 407 K is usually ascribed to desorption of hydrogen from a bulk palladium hydride formed through hydrogen diffusion into Pd crystallites [36]. This behavior is observed when some amount of palladium is present in catalyst as large particles [37], what is in agreement with palladium particle size estimated from CO chemisorption, XRD and TEM.

3.4. Chemisorption studies

Chemisorption measurements allowed determining the Pd dispersion in reduced samples. Red-C-PdSiBEA, red-C-PdSiAlBEA and red-C-PdHAlBEA are characterized by the metal dispersion of 10, 9 and 8 %, and the average Pd particles size (simply calculated from equation reported in [38]) of 11, 13 and 14 nm, respectively. These results are in agreement with results obtained by XRD and TEM (**Table 2**).

3.5. TCE hydrodechlorination

Fig. 4 shows the TCE conversion expressed as C/C_0 versus time of reaction carried out in the presence of red-C-PdSiBEA, red-C-PdSiAlBEA and red-C-PdHAlBEA zeolite

catalysts. Palladium-loaded BEA zeolites are active catalysts in aqueous-phase hydrodechlorination of TCE. The decreasing of pH value (from 6.77 to 3.84) as a function of time indicates that hydrodechlorination process occurs. In the case of all catalysts, after 60 min of reaction almost 90 % of TCE is removed from water. Chromatographic analysis of products formed during TCE HDC in the presence of red-C-PdSiBEA, red-C-PdSiAlBEA and red-C-PdHAlBEA shows mainly formation of non-chlorinated hydrocarbons (ethane and ethene).

A comparative study between red-C-PdSiBEA, red-C-PdSiAlBEA and red-C-PdHAlBEA shows small differences in C/C_0 profiles (**Fig. 4**). The red-C-PdSiBEA indicates higher activity as C/C_0 after 20 min of reaction than red-C-PdSiAlBEA and red-C-PdHAlBEA. The application of red-C-PdSiBEA with the highest Pd dispersion leads to removal almost 80 % of TCE after first 20 min of hydrodechlorination, whereas only 70 and 65 % of TCE is removed by red-C-PdSiAlBEA and red-C-PdHAlBEA, respectively.

These results suggest that the method of Pd-loaded BEA zeolite preparation plays a key role in TCE hydrodechlorination in aqueous-phase. As mentioned in Introduction part, there is some data in the literature concerning structure-sensitivity of aqueous-phases hydrodechlorination [15-20]. For example, Díaz et al. [17] carried out TCE hydrodechlorination in water using 0.5 wt. % Pd supported on: activated carbon (AC), carbon nanofibers (CNF), high surface area graphites (HSAG), alumina and ZSM-5 zeolite. They obtained Pd nanoparticles in the range of 3 – 23 nm for different catalysts. The catalyst containing Pd nanoparticles with size 23 nm (0.5 % Pd/CNF) was found to be the most active in TCE hydrodechlorination.

On the other hand, results obtained by Śrębowata et al. [20] for Pd containing zeolites HZSM-5 and HZSM-5/DeSi indicated the beneficial role of very high Pd dispersion in hydrodechlorination of TCE in aqueous-phase.

Analyzing the literature data [15-20] and the results of our work we assume that both smaller and larger Pd nanoparticles present in red-C-PdSiBEA, red-C-PdSiAlBEA and red-C-PdHAlBEA play a role in aqueous-phase hydrodechlorination of TCE. In the presence of smaller Pd nanoparticles (red-C-PdSiBEA) the reaction occurs faster, but not completely (94 % of TCE conversion after 150 min) probably due to nanoparticles deactivation. The reaction runs slower in the presence of larger nanoparticles (red-C-PdSiAlBEA and red-C-PdHAlBEA), but after 150 min of reaction TCE is almost completely removed.

Hydrodechlorination of TCE over red-C-PdSiBEA, red-C-PdSiAlBEA and red-C-PdHAlBEA is assumed to be pseudo-first-order due to the predominant amount of hydrogen compared to TCE. **Fig. 5** shows the kinetic data according to the linearized pseudo-first-order rate equation. The reaction rate constants k, initial reaction rates r_0 and TOF values are presented in **Table 3**. Our results for red-C-PdSiBEA, red-C-PdSiAlBEA and red-C-PdHAlBEA are comparable to the activity of catalysts with Pd supported on activated carbons, graphite, CeO_2 [39-41], microporous and hierarchical zeolites [20] or CMC-stabilized palladium nanoparticles [42].

3.6. XRD studies

Fig. 6 presents XRD patterns of as prepared samples. X-ray diffractograms of all the samples are similar and characteristic of BEA zeolite. It suggests that crystallinity of BEA zeolite is preserved after different zeolite treatment (dealumination, ion exchange and calcination) and introduction of Pd ions into zeolite structure.

The position of a main narrow diffraction peak near 22.8° changes from 2θ of 22.76° for HAlBEA to 2θ of 22.86° for SiAlBEA and to 2θ of 22.88° for SiBEA. The changes of main diffraction peak position is assigned to lattice contraction/expansion of the BEA structure, as reported earlier [43]. The significant shift to higher 2θ value after dealumination indicates contraction of the matrix as a result of Al removal [44,45].

The introduction of 1 wt. % of Pd into SiBEA zeolite results in a shift of the main diffraction peak from 2θ of 22.88° for SiBEA to 2θ of 22.58° for PdSiBEA. The introduction of Pd into SiAlBEA yields a smaller shift from 2θ of 22.86° for SiAlBEA to 2θ of 22.70° for PdSiAlBEA. The introduction of Pd into HAlBEA does not lead to such significant change in the main diffraction peak position that was observed for SiBEA. In the former case, a small shift from 2θ of 22.76° for HAlBEA to 2θ of 22.66° for PdHAlBEA is observed. These phenomena indicate the expansion of the matrix as a result of the reaction between Pd ions and OH groups of vacant T-atom sites (T = Si or Al) and Pd incorporation into BEA zeolite framework, as it was reported earlier [44, 46-48].

X-ray diffractograms of red-C-PdSiBEA, red-C-PdSiAlBEA and red-C-PdHAlBEA (**Fig. 7**) shows that the crystallinity of BEA zeolite is still preserved after calcination in air and reduction in 10 % H_2/Ar flow, as reported earlier [24,43,49,50]. The characteristic reflection for Pd (111) at 2θ = 40.15° appeared after reduction in all reduced samples.

After calcination and reduction of PdSiBEA, the shift of the main characteristic diffraction peak of BEA zeolite to higher 2θ values is observed (from 2θ of 22.58° for PdSiBEA to 2θ of 22.72° for red-C-PdSiBEA). The contraction of BEA matrix can be explained by Pd output from framework position into extra-framework position and formation of Pd^0 nanoparticles [43]. The reverse effect is noticed for palladium catalysts based on partial dealuminated and non-dealuminated zeolites. In these cases, the main diffraction peak of BEA zeolite is shifted to lower 2θ values (from 2θ of 22.70° for PdSiAlBEA to 2θ of 22.56° for red-C-PdSiAlBEA and from 2θ of 22.76° for PdHAlBEA to 2θ of 22.36° for red-C-PdHAlBEA). This shift can be explained by presence in both PdSiAlBEA and PdHAlBEA samples mainly extra-framework Pd(II) species and their calcination could lead to incorporation of part of this extra-framework Pd(II) species in framework position with expansion of the BEA matrix and treatment with H_2 at 873 K involve formation of Pd^0

nanoparticles in extra-framework position of red-C-PdSiAlBEA and red-C-PdHAlBEA mainly from extra-framework Pd(II) species. Similar results were observed for other metal-loaded BEA zeolites [43].

XRD results obtained for catalysts after reduction and after hydrodechlorination of TCE show that the crystal structure of BEA is preserved (**Fig. 7**). For catalysts based on SiBEA and SiAlBEA supports inverse shift of the main diffraction peak after reaction with TCE is observed from 2θ of 22.72° for red-C-PdSiBEA to 2θ of 22.86° for spent-red-C-PdSiBEA and from 2θ of 22.56° for red-C-PdSiAlBEA to 2θ of 22.40° for spent-red-C-PdSiAlBEA. These inverse effects can be explained by partial removal of Pd from framework of red-C-PdSiBEA and partial oxidation of extra-framework Pd nanoparticles of red-C-PdSiAlBEA upon hydrochlorination of TCE with formation of Pd(II) species which can migrate and incorporate into zeolite framework in reaction condition [51]. The shift of main diffraction peak from 2θ of 22.36° for red-C-PdHAlBEA to 2θ of 22.52° for spent-red-C-PdHAlBEA is probably a result of carbon species formation and/or irreversible adsorption of HCl occurred in the zeolite [52, 53].

3.7. TEM studies

TEM measurements allowed to determine the Pd particles size distribution in red-C-PdSiBEA, red-C-PdSiAlBEA and red-C-PdHAlBEA. All samples reduced at 873 K for 3 h are characterized by the dispersion of 10-14 % and the average Pd particle size in the range of 8-14 nm (**Table 2**). These values are in very good agreement with chemisorption and XRD results (**Table 2**).

TEM images of red-C-PdSiBEA, red-C-PdSiAlBEA and red-C-PdHAlBEA and palladium particles size distributions are shown in **Fig. 8a, 9a** and **10a**. The presented histograms exhibit rather uniform distribution of metallic nanoparticles. In all catalysts, Pd is very good dispersed in zeolite material. The average nanoparticles sizes are similar for all

catalysts (**Table 2**). However, almost 47 % of small nanoparticles (1 – 6 nm) is present in red-C-PdSiBEA (**Fig. 8a**), whereas only 36 and 34 % is present in red-C-SiAlBEA (**Fig. 9a**) and red-C-HAlBEA (**Fig. 10a**), respectively. This means that the way of catalysts preparation has an impact on metal particles diameter and particles distribution. Smaller Pd nanoparticles after reduction step are obtained due to the impregnation of completely dealuminated BEA zeolite (SiBEA) by $PdCl_2$ aqueous solution and incorporation of Pd ions into zeolite structure in framework position. However, after impregnation of partially dealuminated (SiAlBEA) and non-dealuminated (HAlBEA) zeolites by $PdCl_2$ aqueous solution, Pd ions are introduced mainly in extra-framework position what gives after reduction step larger metal particles, in particular in red-C–PdHAlBEA.

TEM images, palladium particles size distribution and XRD results for catalysts after reaction (**Table 2**, **Fig. 8b**, **9b** and **10b**) show that Pd nanoparticles are slightly larger than that observed in the case of catalysts after reduction step, what can be associated with migration and agglomeration of metal particles during reaction.

4. Conclusions

In this work we have shown that the method of catalysts synthesis has the influence on the distribution of Pd nanoparticles and impact on their catalytic activity in aqueous-phase hydrodechlorination of TCE.

The two-step postsynthesis method and full dealumination of BEA zeolite allowed obtaining the smallest and most active Pd nanoparticles (removal of 80 % TCE after 20 min of reaction) as opposed to the conventional wet impregnation (removal only of 65 % TCE after the same time).

Acknowledgements

This work was partially financed by Grant No. 2011/03/D/ST5/05516 from the National Science Centre, Poland. The synthesis and partially characterization of Pd-loaded BEA zeolites were carried out within GDRI PAN-CNRS program (Catalysis for Environment: Depollution, Renewable Energy and Clean Fuels).

References

[1] Bouriazos A., Sotiriou S., Stathis P., Papadogianakis G., Appl. Catal. B, 150-151 (2014) 345-353

[2] Yuan T., Gong H., Kailasam K., Zhao Y., Thomas A., Zhu J., J. Catal., 326 (2015) 38-42

[3] Figueira C.A., Lopes P.S., Gomes P.T., Tetrahedron, 71 (2015) 4362-4371

[4] Akbayrak S., Kaya M., Volkan M., Özkar S., Appl. Catal. B, 147 (2014) 387-393

[5] Kim J., Zhang P., Li J., Wang J., Fu P., Chem. Eng. J, 252 (2014) 337-345

[6] Chen M., Qi L., Fan L., Zhou R., Zheng X., Mater. Lett., 62 (2008) 3646-3648

[7] Anulewicz P.A., White R.F., Martin B.M., Winter M.R., Weinberg J.M., Vieira V., Aschengrau A., Neurotoxicol. Teratol., 34 (2012) 350-359

[8] Rusyn I., Chiu W.A., Lash L.H., Kromhout H., Hansen J., Guyton K.Z., Pharmacol. Therap., 141 (2014) 55-68

[9] Guha N., Loomis D., Grosse Y., Lauby-Secretan B., El Ghissassi F., Bouvard V., Benbrahim-Tallaa L., Baan R., Mattock H., Straif K., Lancet Oncol., 13 (2012) 1192-1193

[10] Han Y., Gu G., Sun J., Wang W., Wan H., Xu Z., Zheng Sh., Appl. Surf. Sci., 355 (2015) 183-190

[11] Zhang M., Bacik D.B., Roberts Ch.B., Zhao D., Water Res., 47 (2013) 3706-3715

[12] Navon R., Eldad Sh., Mackenzie K., Kopinke F.-D., Appl. Catal. B, 119-120 (2012) 241-247

[13] Park J., Joo J., Kwon S.G., Jang Y., Hyeon T., Angew. Chem., Int. Ed., 46 (2007), 4630-4660

[14] Baeza J.A., Calvo L., Gilarranz M.A., Mohedano A.F., Casas J.A., Rodriguez J.J., J. Catal., 293 (2012) 85-93

[15] Juszczyk W., Malinowski A., Karpiński Z., Appl. Catal. A., 166 (1998) 311-319

[16] Aramendía M.A., Boráu V., García I.M., Jiménez C., Lafont F., Marinas A., Marinas J.M., Urbano F.J., J. Catal., 187 (1999) 392–399

[17] Díaz E., McCall A., Faba L., Sastre H., Ordonez S., Environ. Prog. Sustainable Energy, 32 (2013) 1217–1222

[18] Gómez-Quero S., Cárdenas-Lizana F., Keane M.A., Ind. Eng. Chem. Res., 47 (2008), 6841–6853

[19] Dong Z., Le X., Liu Y., Dong Ch., Ma J., J. Mater. Chem. A, 2 (2014) 18775-18785

[20] Śrębowata A., Tarach K., Girman V., Góra-Marek K., Appl. Catal. B, 181 (2016) 550–560

[21] Ardila A.N., Reyes J., Arriola E., Hernández J.A., Fuentes G.A., Appl. Catal. A, 497 (2015) 211-215

[22] Imre B., Hannus I., Kiricsi I., J. Mol. Struct., 744–747 (2005) 501-506

[23] Hannus I., Főző M., Halász J., Tasi G., Stud. Surf. Sci. Catal., 158 (2005) 1803-1810

[24] Śrębowata A., Baran R., Łomot D., Lisovytskiy D., Onfroy T., Dzwigaj S., Appl. Catal. B, 147 (2014) 208-220

[25] Śrębowata A., Kamińska I.I., Giziński D., Wideł D., Oszczudłowski J., Catal. Today, 251 (2015) 60-65

[26] Novak Tusar N., Mali G., Arcon I., Kaucic V., Ghanbari-Siahkali A., Dwyer J., Micropor. Mesopor. Mater., 55 (2002) 203–216

[27] Roldán R., Beale A.M., Sánchez-Sánchez M., Romero-Salguero F.J., Jiménez-Sanchidrián C., Gómez J.P., Sankar G., J. Catal., 254 (2008) 12-26

[28] Zhang Z., Sachtler W.M.H., Zeolites, 10 (1990) 784-789

[29] Okitsu K., Bandow H., Maeda Y., Chem. Mater., 8 (1996) 315-317

[30] Shimizu K., Maruyama R., Komai S., Kodama T., Kitayama Y., J. Catal., 227 (2004) 202-209

[31] Celebi M., Yurderi M., Bulut A., Kaya M., Zahmakiran M., Appl. Catal. B, 180 (2016) 53-64

[32] Boroń P., Chmielarz L., Gil B., Marszałek B., Dzwigaj S., Appl. Catal. B, 198 (2016) 457–470

[33] Kyriienko P.I., Larina O V., Popovych N.O., Soloviev S.O., Millot Y., Dzwigaj S., J. Mol. Catal. A: Chem., 424 (2016) 27-36

[34] Yang K., Wang B., Chen L., Wang X., Catal. Commun., 9 (2008) 431-436

[35] Bendahou K., Cherif L., Siffert S., Tidahy H.L., Benaïssa H., Aboukaïs A., Appl. Catal. A, 351 (2008) 82-87

[36] Vannice M.A., Chou P., J. Catal., 107 (1987) 129-139

[37] Echeandia S., Pawelec B., Barrio V.L., Arias P.L., Cambra J.F., Loricera C.V., Fierro J.L.G., Fuel, 117 (2014) 1061-1073

[38] Ichikawa S., Poppa H., Boudart M., J. Catal. 91 (1985) 1-10

[39] Cobo M., Becerra J., Costelblanco M., Cifuentes B., Conesa J.A., J. Environ. Menag., 158 (2015) 1-10

[40] Molina C.B., Pizarro A.H., Casas J.A., Rodrigues J.J., Appl. Catal. B, 148-149 (2014) 330-338

[41] Díaz E., Faba L., Ordóñez S. Appl. Catal. B, 104 (2011) 415–417

[42] Zhang M., Bacik D.B., Roberts Ch.B., Zhao D., Water Res., 47 (2013), 3706–3715

[43] Śrębowata A., Baran R., Casale S., Kamińska I.I., Łomot D., Lisovytskiy D., Dzwigaj S., Appl. Catal. B, 152–153 (2014) 317-327

[44] Dzwigaj S., Peltre M.J., Massiani P., Davidson A., Che M., Sen T., Sivasanker S., Catal. Comm., 87 (1988)

[45] Dzwigaj S., Matsuoka M., Franck R., Anpo M., Che M., J. Phys. Chem. B, 102 (1998) 6309-6312

[46] Dzwigaj S., Massiani P., Davidson A., Che M., J. Mol. Catal. A: Chem., 155 (2000) 169-182

[47] Dzwigaj S., Janas J., Gurgul J., Socha R.P., Shishido T., Che M., Appl. Catal. B, 85 (2009) 131-138

[48] Janas J., Gurgul J., Socha R.P., Kowalska J., Nowinska K., Shishido T., Che M., Dzwigaj S., J. Phys. Chem. C, 113 (2009) 13273-13281

[49] Śrębowata A., Baran R., Kamińska I.I., Onfroy T., Krafft J.-M., Dzwigaj S., Catal. Today, 251 (2015) 73-80

[50] Śrębowata A., Zielińska I., Baran R., Słowik G., Dzwigaj S., Catal. Comm., 69 (2015) 154-160

[51] Śrębowata A., Baran R., Lisovytskiy D., Kamińska I.I., Dzwigaj S., Catal. Comm., 57 (2014) 107-110

[52] Hannus I., Appl. Catal. A, 189 (1999) 263–276

[53] Shalygin A.S., Malysheva L.V., Paukshtis E.A., Kinet. Catal., 52 (2011) 305-315

Table 1. Specific surfaces areas and pore volumes determined from the nitrogen adsorption–desorption isotherms of calcined zeolites and catalysts.

Sample	BET specific surface area ($m^2\ g^{-1}$)	Micropore volume ($cm^3\ g^{-1}$)	Mesopore volume ($cm^3\ g^{-1}$)	Total pore volume ($cm^3\ g^{-1}$)
C-SiBEA	374	0.12	0.04	0.16
C-PdSiBEA	393	0.13	0.03	0.16
C-SiAlBEA	310	0.09	0.03	0.15
C-PdSiAlBEA	447	0.10	0.06	0.16
C-HAlBEA	329	0.10	0.03	0.13
C-PdHAlBEA	377	0.10	0.04	0.14

Table 2. Palladium particle sizes estimated from CO chemisorption, XRD and TEM measurements.

Sample	Palladium particle size (nm) estimated from			Dispersion[b] (%)
	CO chemisorption	XRD	TEM[a]	
red-C-PdSiBEA	11	10	8	14
spent-red-C-PdSiBEA	-	17	9	12
red-C-PdSiAlBEA	13	10	9	12
spent-red-C-PdSiAlBEA	-	10	9	12
red-C-PdHAlBEA	14	10	9	12
spent-red-C-PdHAlBEA	-	10	11	10

[a] the average distribution of Pd nanoparticles

[b] calculated form equation D (%) = (1.12/d) × 100%, where d (nm) is the average Pd nanoparticles size estimated from TEM measurements [41]

Table 3. The reaction rate constant k, coefficient of determination R^2, initial reaction rate r_0 and TOF values for hydrodechlorination of TCE at 303 K on PdBEA zeolites.

Sample	k[a] (min^{-1})	R^2	r_0[b] (mol s^{-1} g_{Pd}^{-1}) × 10^{-4}	TOF[c] (s^{-1}) × 10^{-2}
red-C-PdSiBEA	0.1365	0.9406	2.56	19.45
red-C-PdSiAlBEA	0.0907	0.9364	2.11	18.67
red-C-PdHAlBEA	0.0707	0.8083	1.76	15.61

[a] the reaction rate constant k calculated from equation $\ln(C/C_0) = -kt$, where k is first-order rate constant (min^{-1}) and t is reaction time (min)

[b] the initial reaction rate calculated from equation: r_0 (mol s^{-1} g_{Pd}^{-1}) = $(n_{t=0} - n_{t=600})/(\Delta t \times m_{Pd})$, where $n_{t=0}$ (mol) – the initial amount of TCE moles, $n_{t=600}$ (mol) – amount of TCE moles after 600 seconds of reaction, Δt (s) = 600 – initial reaction time, m_{Pd} (g) – mass of Pd in the catalyst [39]

[c] TOF calculated from equation: TOF (s^{-1}) = $(r_0 \times M \times 100)/D$, where r_0 (mol s^{-1} g_{Pd}^{-1}) – the initial reaction rate, M (g mol^{-1}) – atomic mass of Pd, D (%) – metal dispersion [40]

Figure captions:

Fig. 1. DR UV-Vis spectra recorded at ambient atmosphere of as prepared SiBEA, PdSiBEA, SiAlBEA, PdSiAlBEA, HAlBEA and PdHAlBEA.

Fig. 2. Adsorption and desorption isotherms of N_2 at 77 K of calcined C-SiBEA, C-PdSiBEA, C-SiAlBEA, C-PdSiAlBEA, C-HAlBEA and C-PdHAlBEA. Empty symbols: adsorption; full symbols: desorption.

Fig. 3. TPR patterns of calcined C-PdSiBEA, C-PdSiAlBEA and C-PdHAlBEA.

Fig. 4. Kinetics of TCE hydrodechlorination at 303 K in the presence of red-C-PdSiBEA, red-C-PdSiAlBEA and red-C-PdHAlBEA.

Fig. 5. Plots of $\ln(C/C_0)$ versus reaction time for hydrodechlorination of TCE at 303 K on red-C-PdSiBEA, red-C-PdSiAlBEA and red-C-PdHAlBEA.

Fig. 6. XRD patterns recorded at ambient atmosphere of as prepared SiBEA, PdSiBEA, SiAlBEA, PdSiAlBEA, HAlBEA and PdHAlBEA recorded at ambient atmosphere.

Fig. 7. XRD patterns recorded at ambient atmosphere of samples after reduction (red-C-PdSiBEA, red-C-PdSiAlBEA and red-C-PdHAlBEA) and after reaction with TCE (spent-red-C-PdSiBEA, spent-red-C-PdSiAlBEA and spent-red-C-PdHAlBEA).

Fig. 8. TEM images and Pd particle size distribution of a) red-C-PdSiBEA and b) spent-red-C-PdSiBEA.

Fig. 9. TEM images and Pd particle size distribution of a) red-C-PdSiAlBEA and b) spent-red-C-PdSiAlBEA.

Fig. 10. TEM images and Pd particle size distribution of a) red-C-PdHAlBEA and b) spent-red-C-PdHAlBEA.

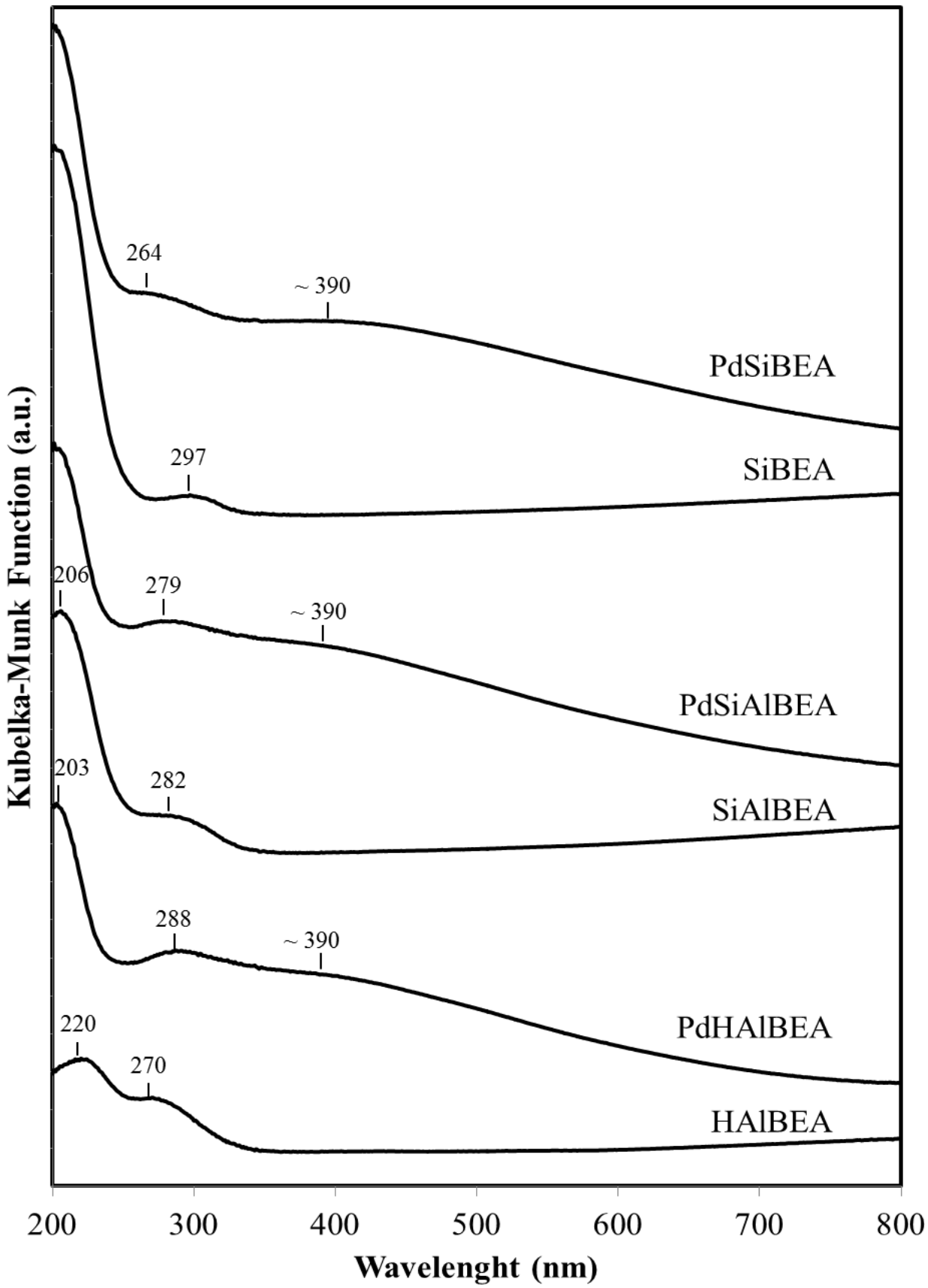
Kubelka-Munk Function (a.u.)
264
~ 390
PdSiBEA
297
SiBEA
206
279
~ 390
PdSiAlBEA
203
282
SiAlBEA
288
~ 390
PdHAlBEA
220
270
HAlBEA
200
300
400
500
600
700
800
Wavelenght (nm)

Fig. 1.

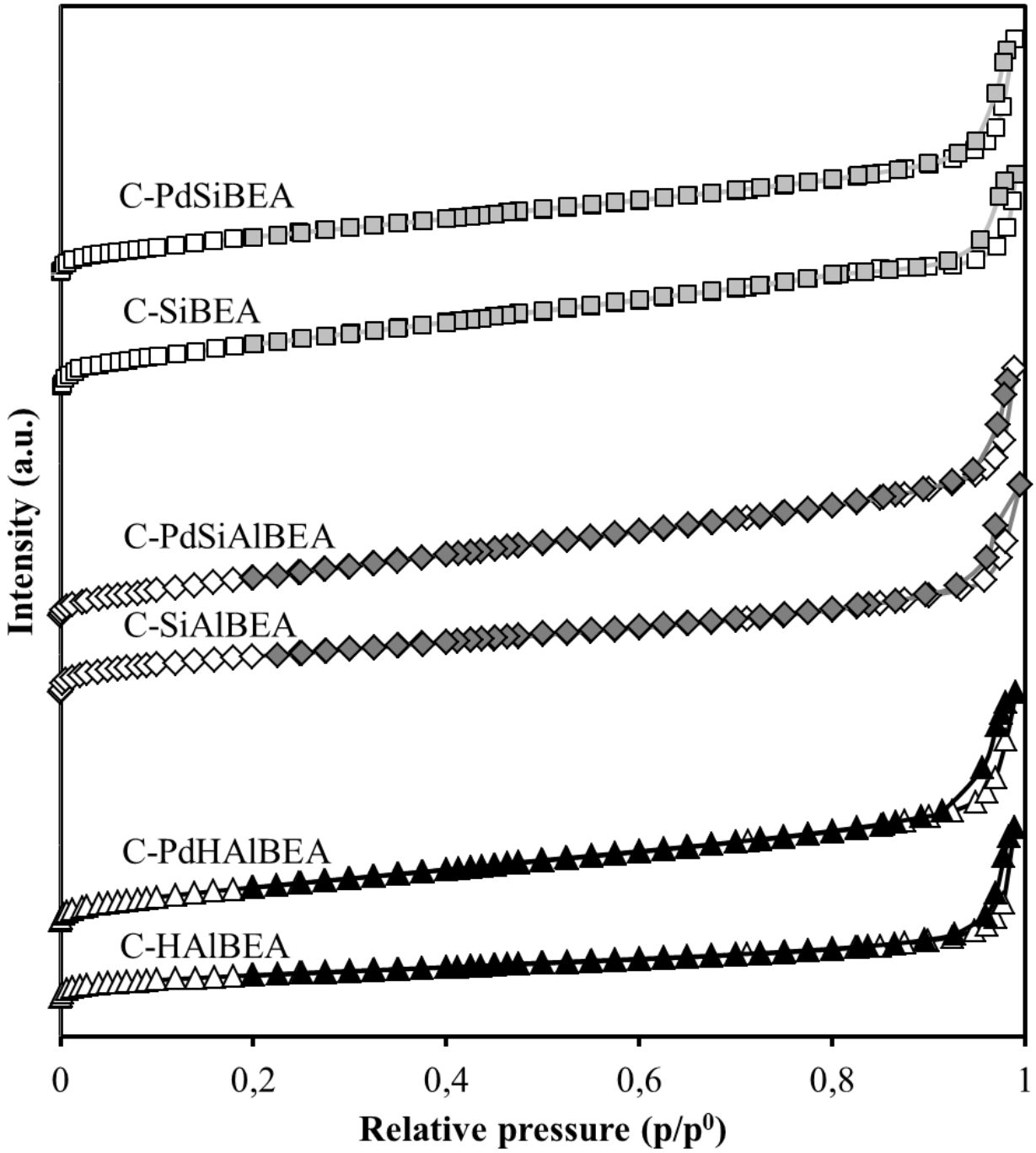
C-PdSiBEA
C-SiBEA
C-PdSiAlBEA
C-SiAlBEA
C-PdHAlBEA
C-HAlBEA
Intensity (a.u.)
0
0,2
0,4
0,6
0,8
1
Relative pressure (p/p0)

Fig. 2.

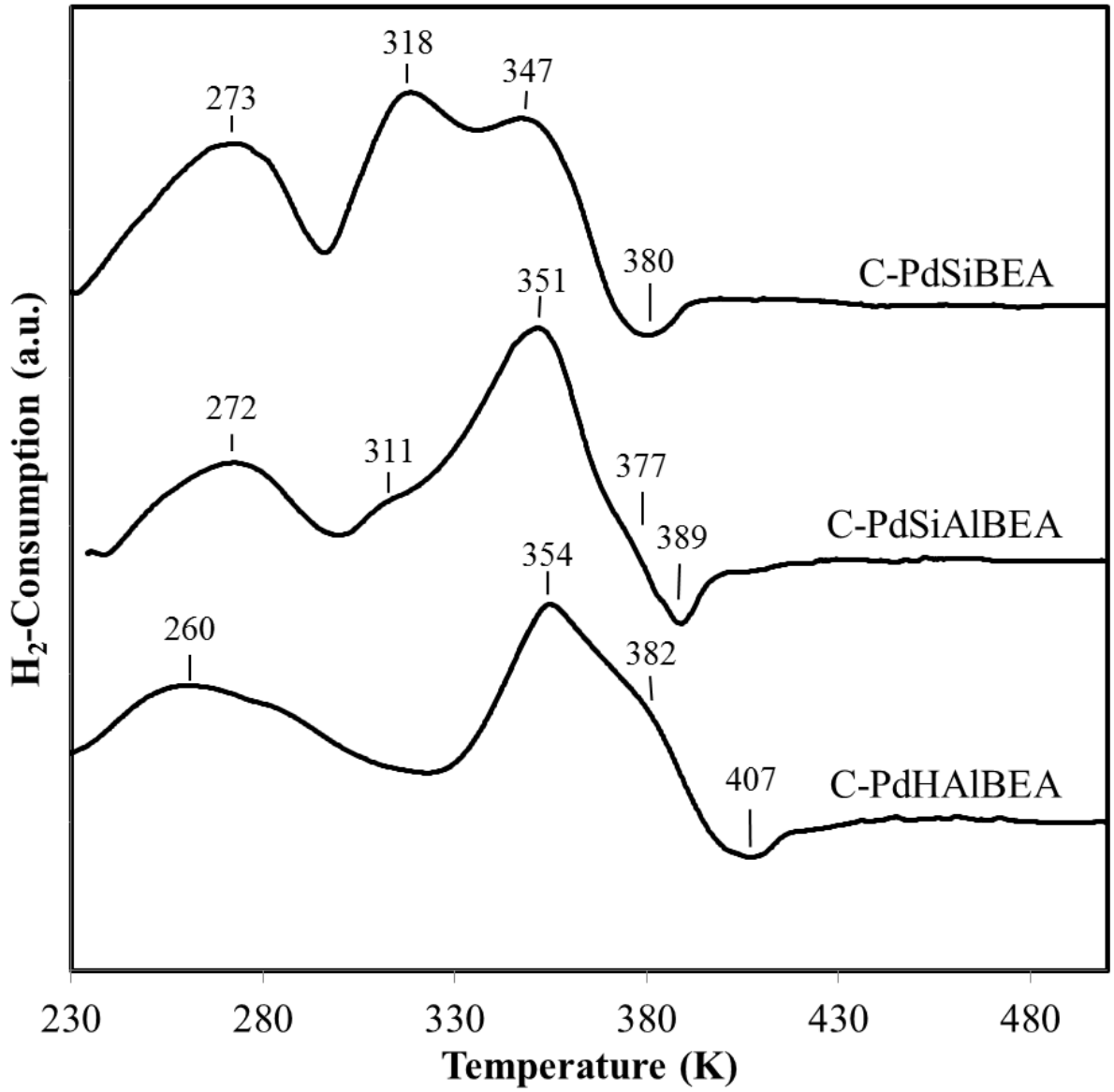
318
347
273
380
C-PdSiBEA
351
272
311
377
389
C-PdSiAlBEA
354
260
382
407
C-PdHAlBEA
H2-Consumption (a.u.)
230
280
330
380
430
480
Temperature (K)

Fig. 3.

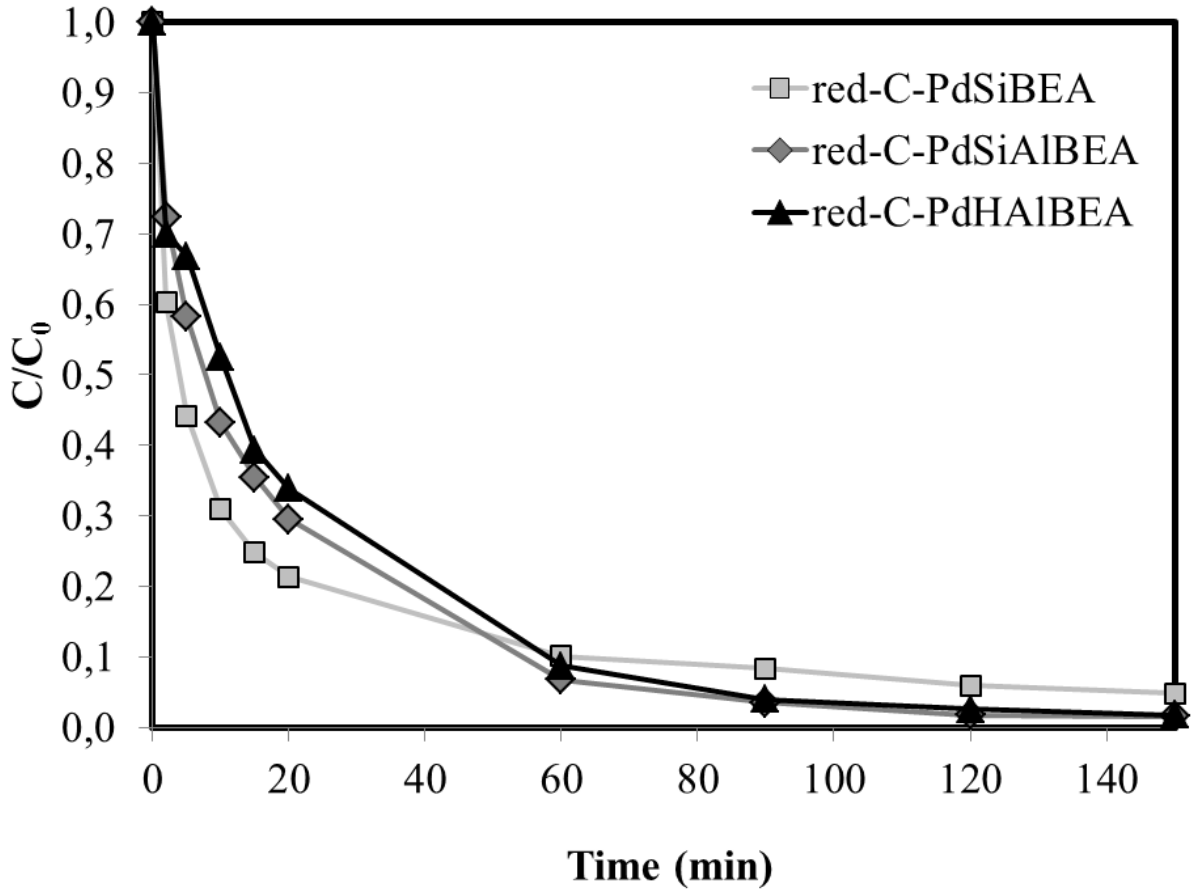
1,0
0,9
0,8
0,7
0,6
0,5
0,4
0,3
0,2
0,1
0,0
C/C0
0
20
40
60
80
100
120
140
Time (min)
red-C-PdSiBEA
red-C-PdSiAlBEA
red-C-PdHAlBEA

Fig. 4.

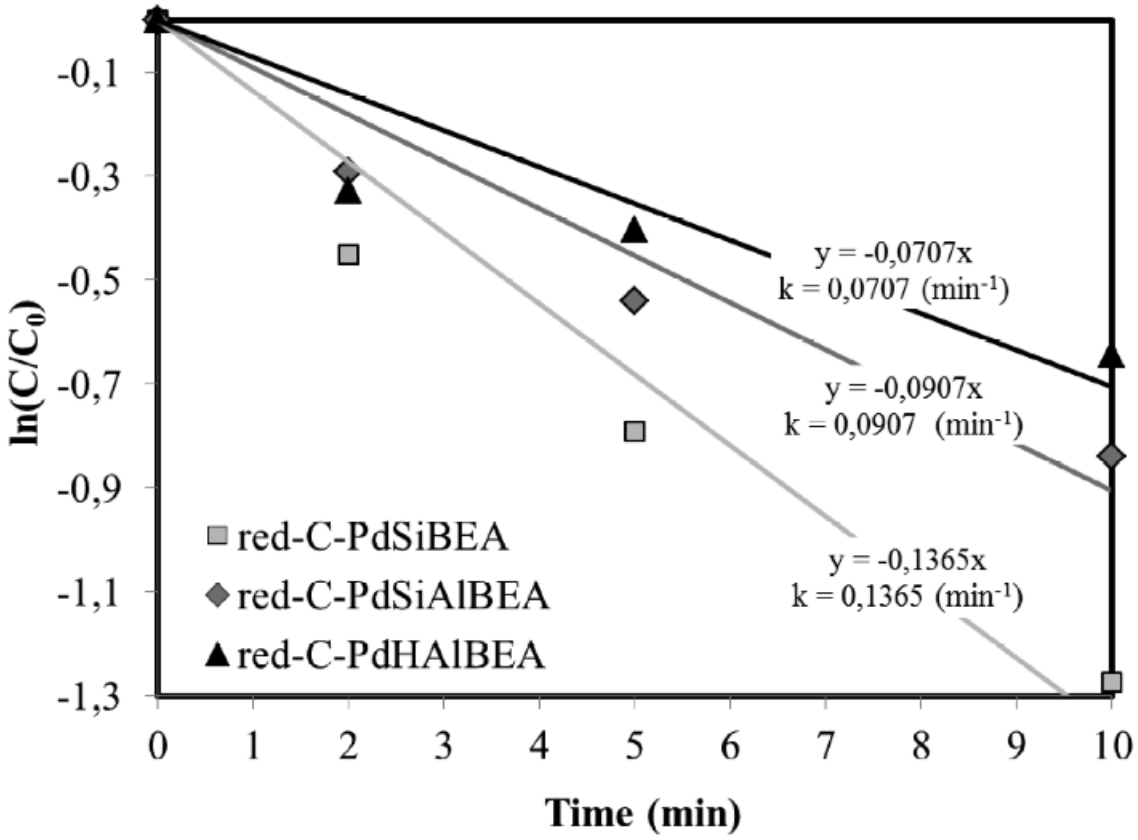
-0,1
-0,3
-0,5
-0,7
-0,9
-1,1
-1,3
ln(C/C0)
0
1
2
3
4
5
6
7
8
9
10
Time (min)
y = -0,0707x
k = 0,0707 (min-1)
y = -0,0907x
k = 0,0907 (min-1)
y = -0,1365x
k = 0,1365 (min-1)
red-C-PdSiBEA
red-C-PdSiAlBEA
red-C-PdHAlBEA

Fig. 5.

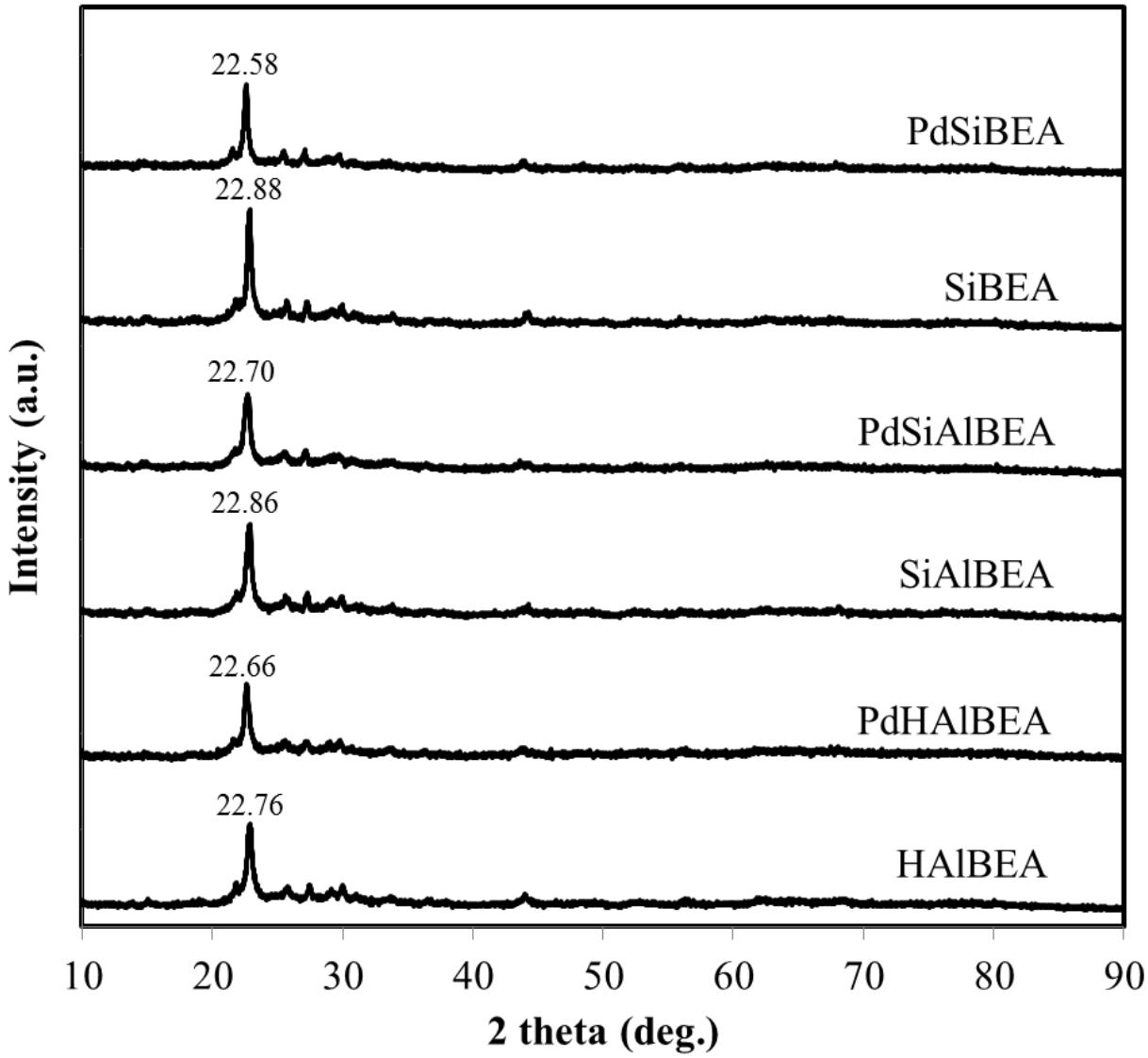
22.58
PdSiBEA
22.88
SiBEA
22.70
PdSiAlBEA
22.86
SiAlBEA
22.66
PdHAlBEA
22.76
HAlBEA
Intensity (a.u.)
10
20
30
40
50
60
70
80
90
2 theta (deg.)

Fig. 6.

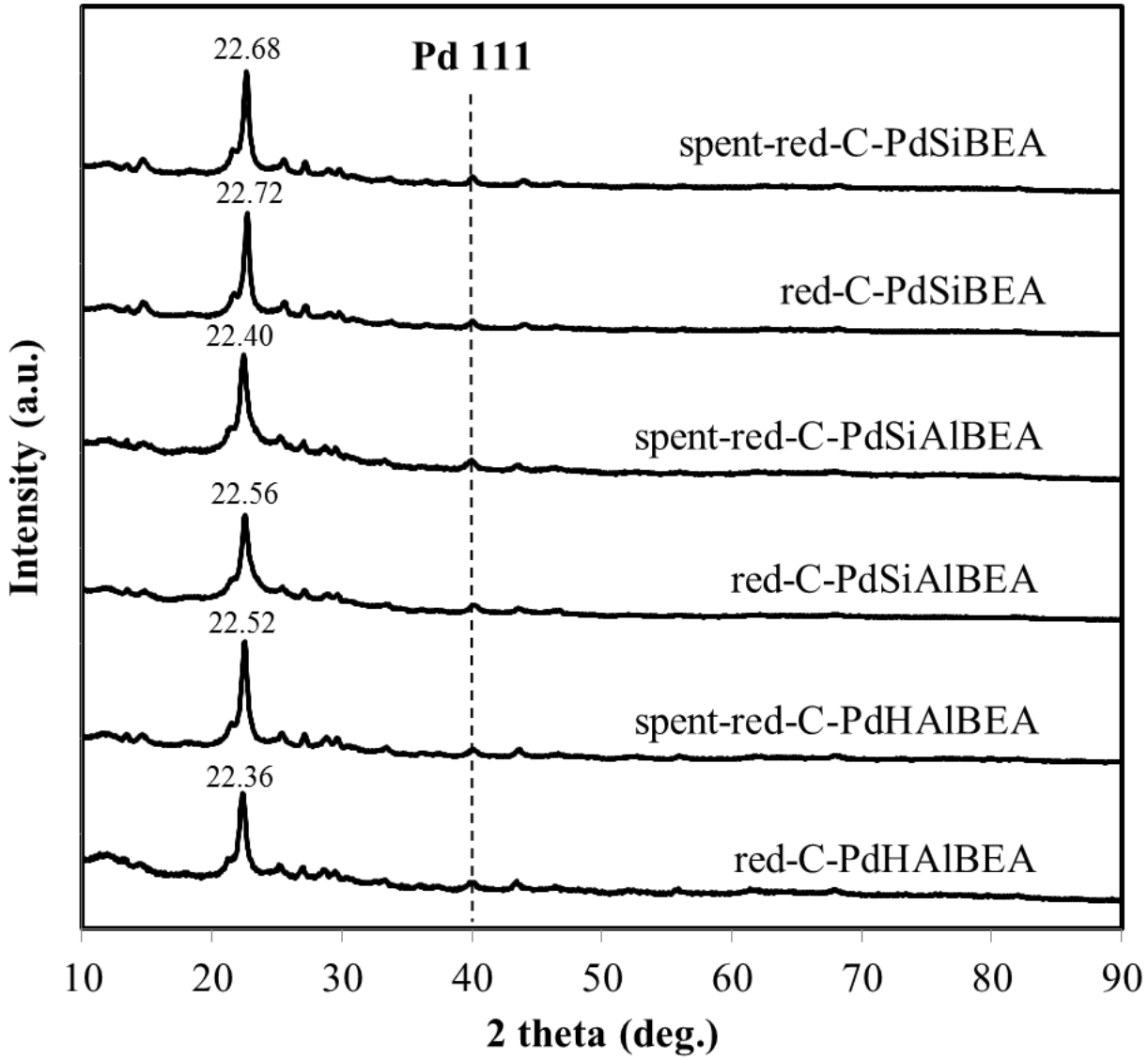
Pd 111
22.68
spent-red-C-PdSiBEA
22.72
red-C-PdSiBEA
22.40
spent-red-C-PdSiAlBEA
22.56
red-C-PdSiAlBEA
22.52
spent-red-C-PdHAlBEA
22.36
red-C-PdHAlBEA
Intensity (a.u.)
10
20
30
40
50
60
70
80
90
2 theta (deg.)

Fig. 7.

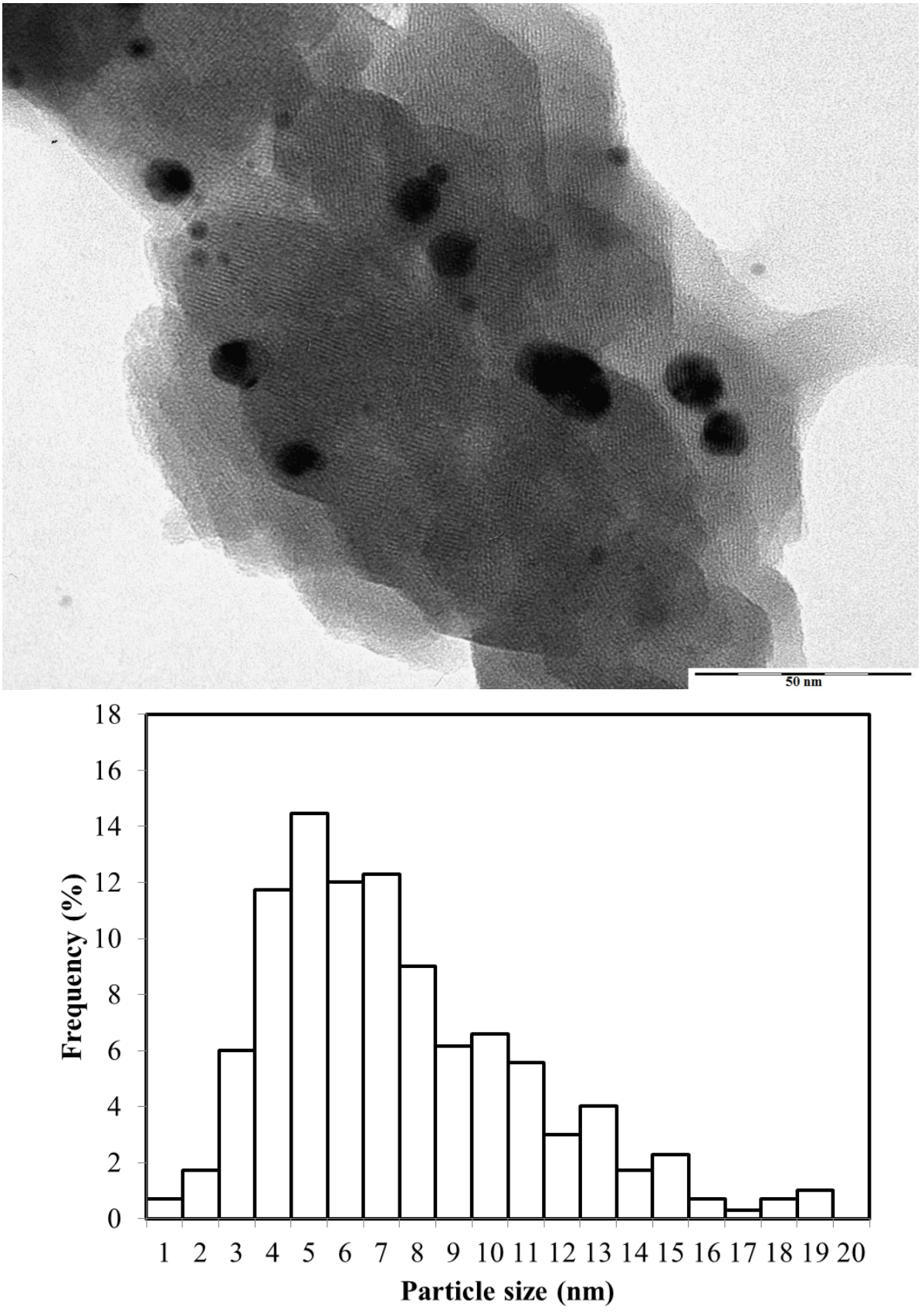
50 nm
Frequency (%)
0
2
4
6
8
10
12
14
16
18
1 2 3 4 5 6 7 8 9 10 11 12 13 14 15 16 17 18 19 20
Particle size (nm)

Fig. 8a

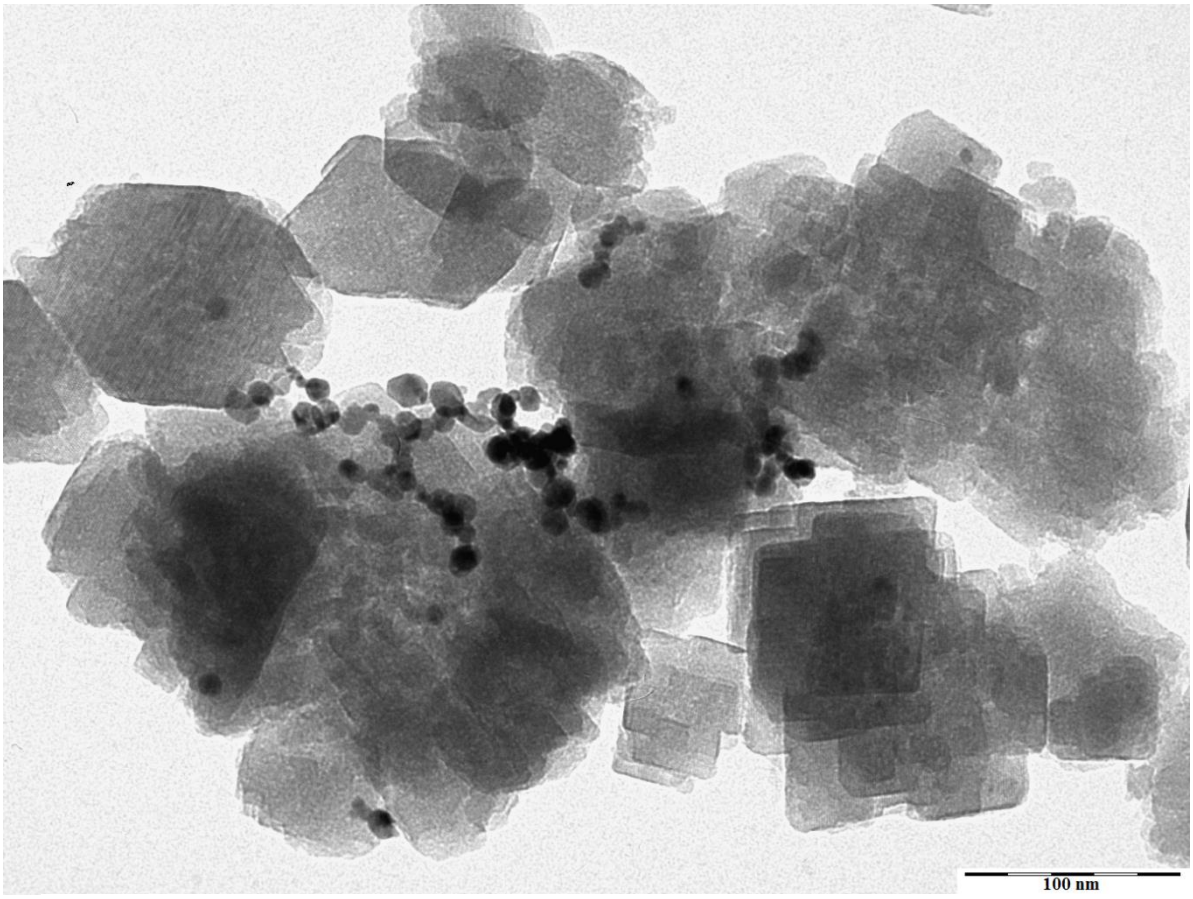
100 nm

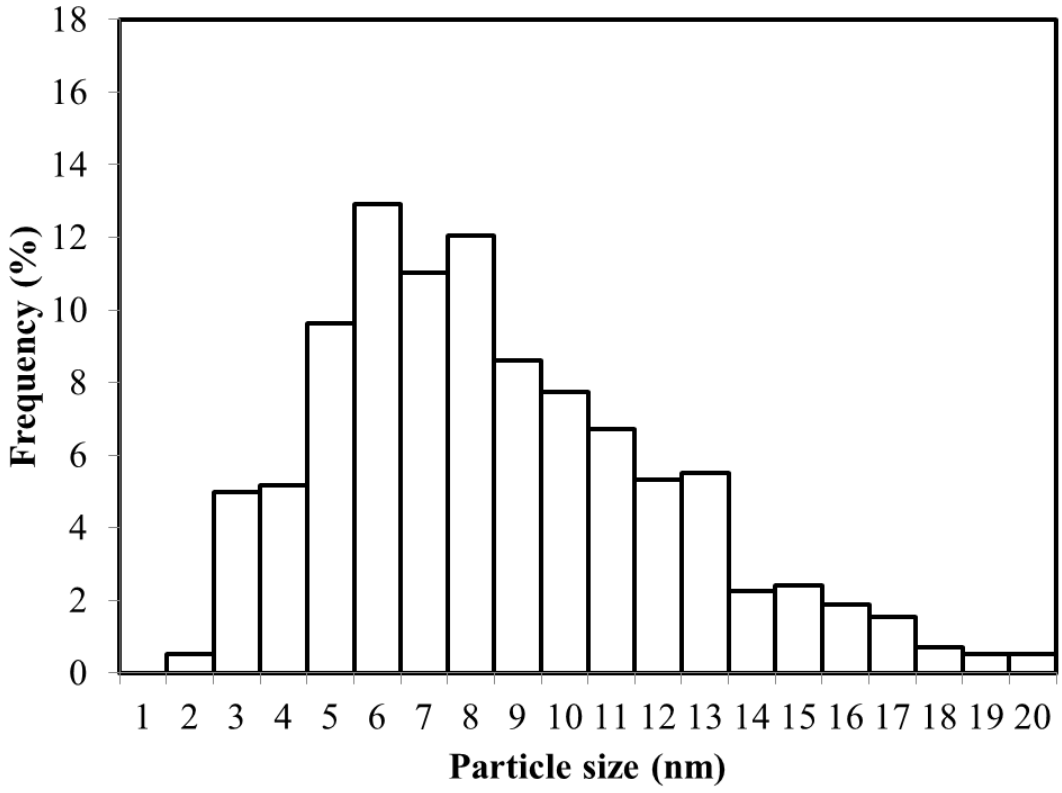
Frequency (%)
0
2
4
6
8
10
12
14
16
18
1 2 3 4 5 6 7 8 9 10 11 12 13 14 15 16 17 18 19 20
Particle size (nm)

Fig. 8b

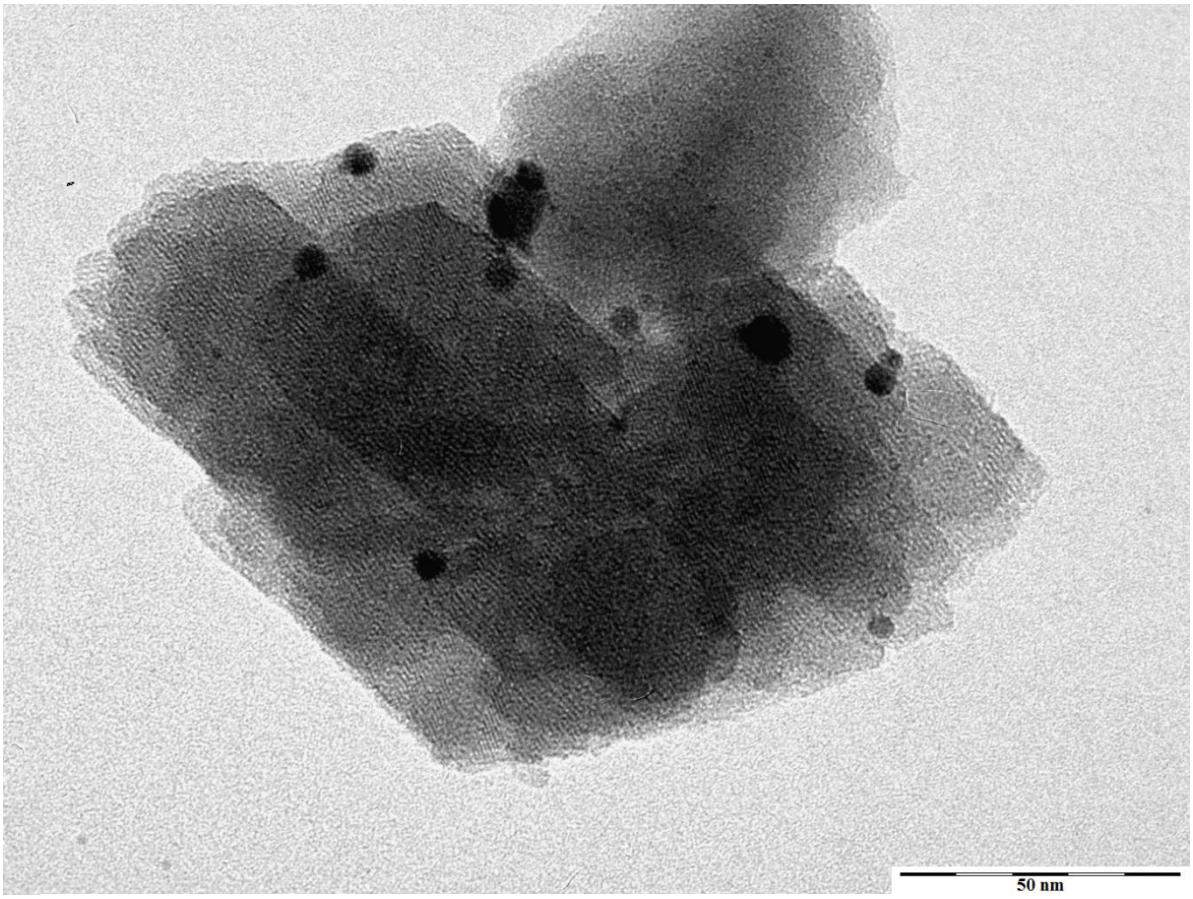
50 nm

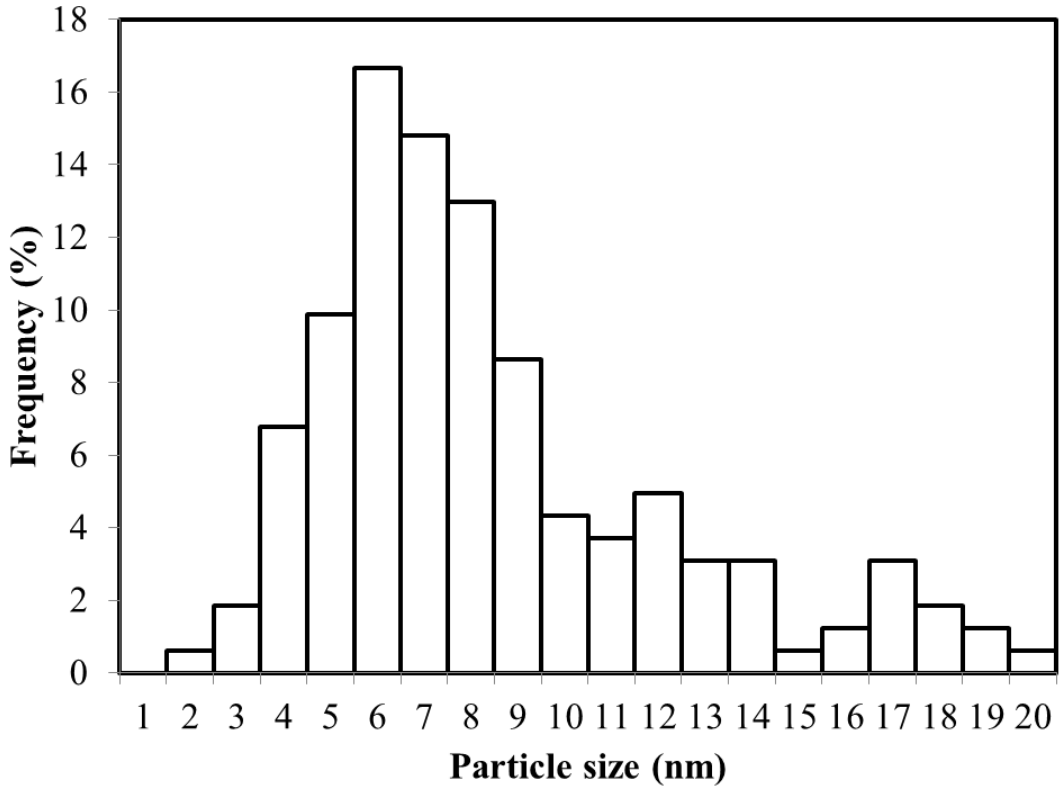
Frequency (%)
0
2
4
6
8
10
12
14
16
18
1 2 3 4 5 6 7 8 9 10 11 12 13 14 15 16 17 18 19 20
Particle size (nm)

Fig. 9a

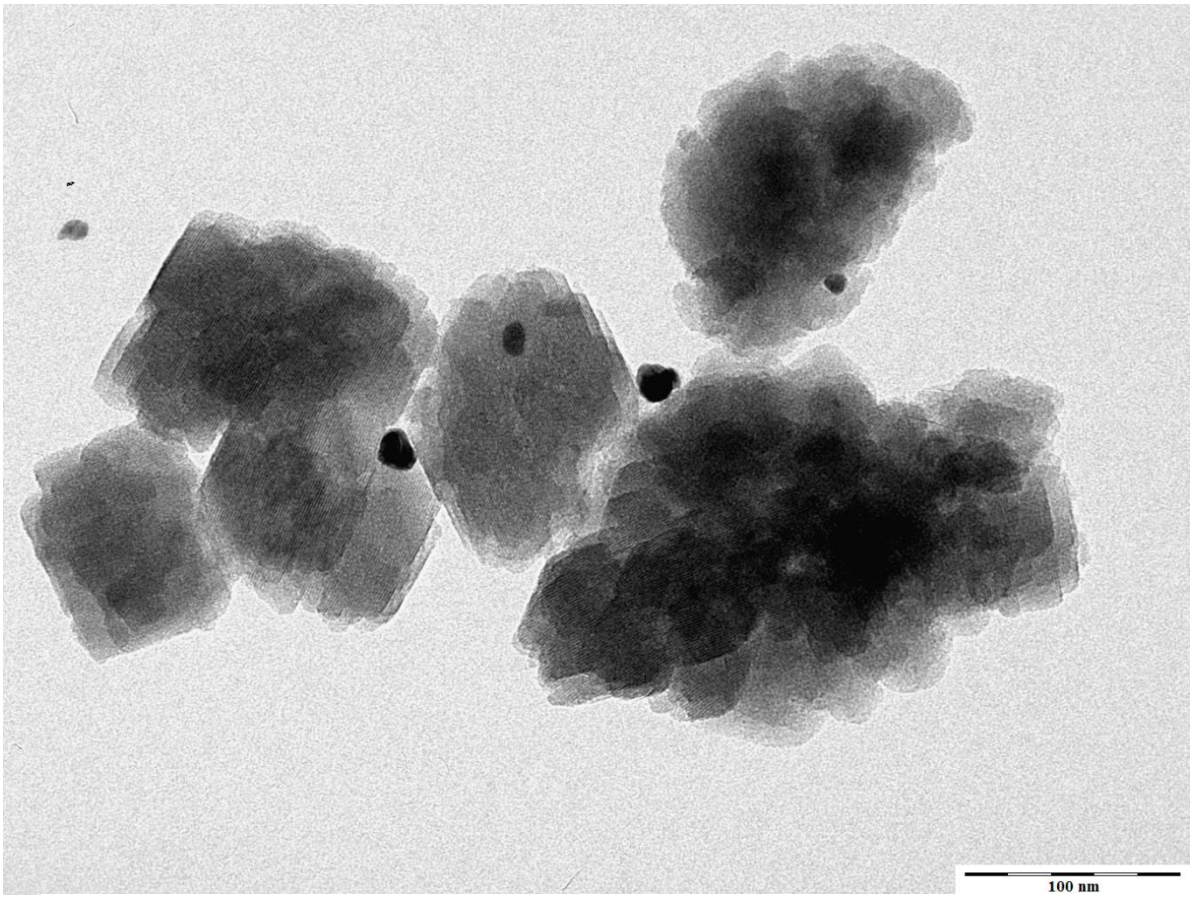
100 nm

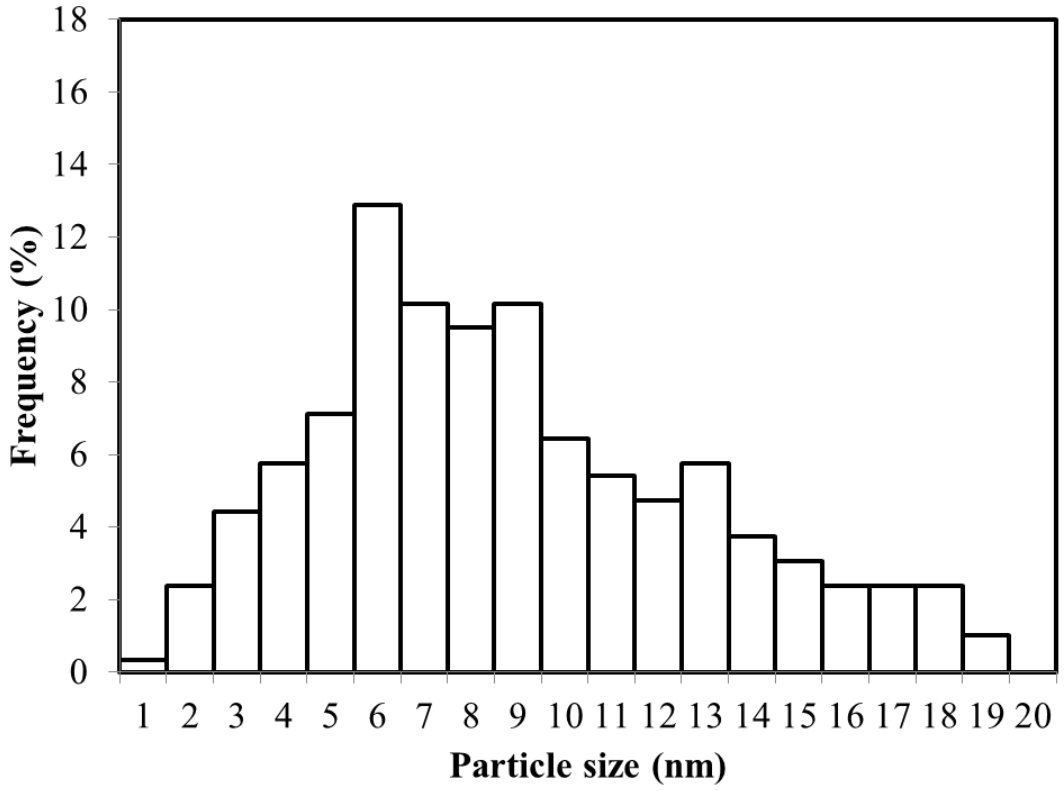
Frequency (%)
0
2
4
6
8
10
12
14
16
18
1 2 3 4 5 6 7 8 9 10 11 12 13 14 15 16 17 18 19 20
Particle size (nm)

Fig. 9b

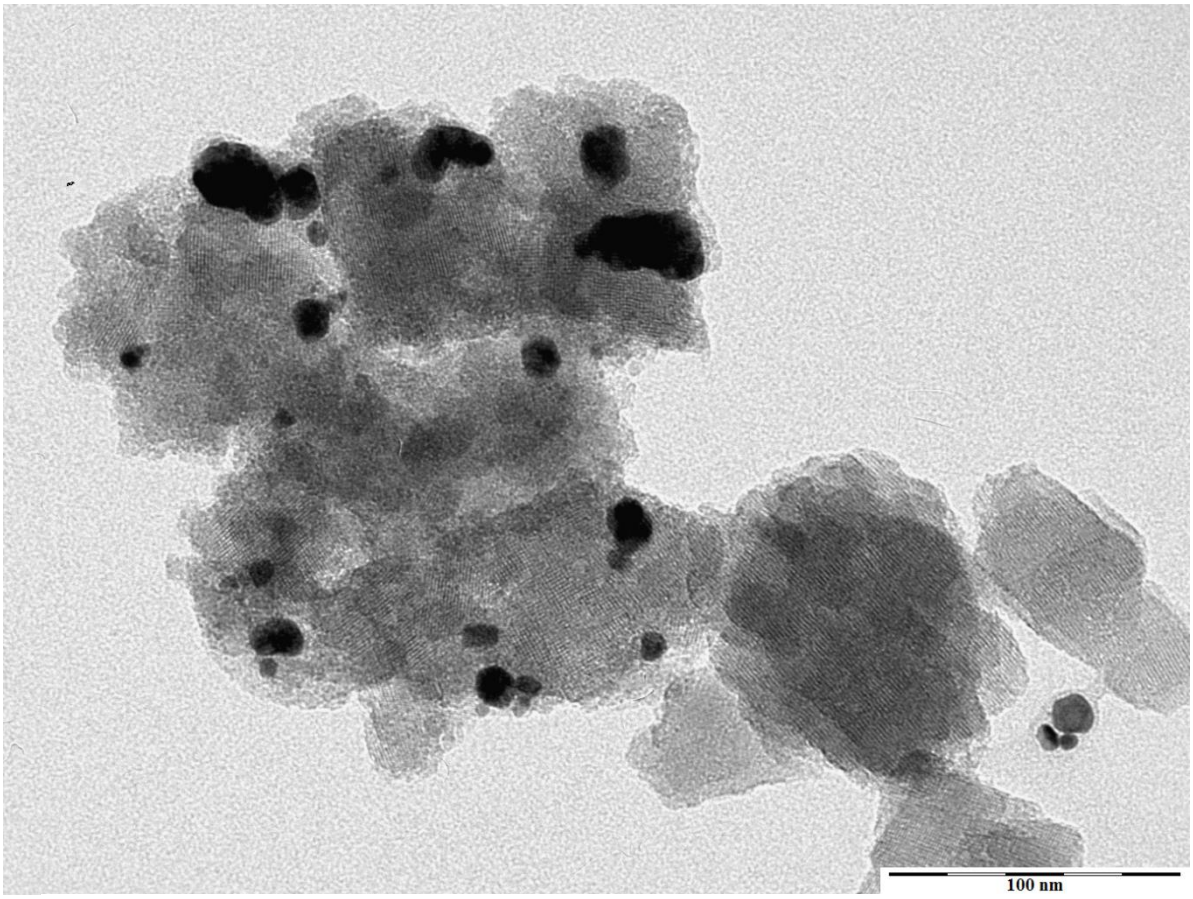
100 nm

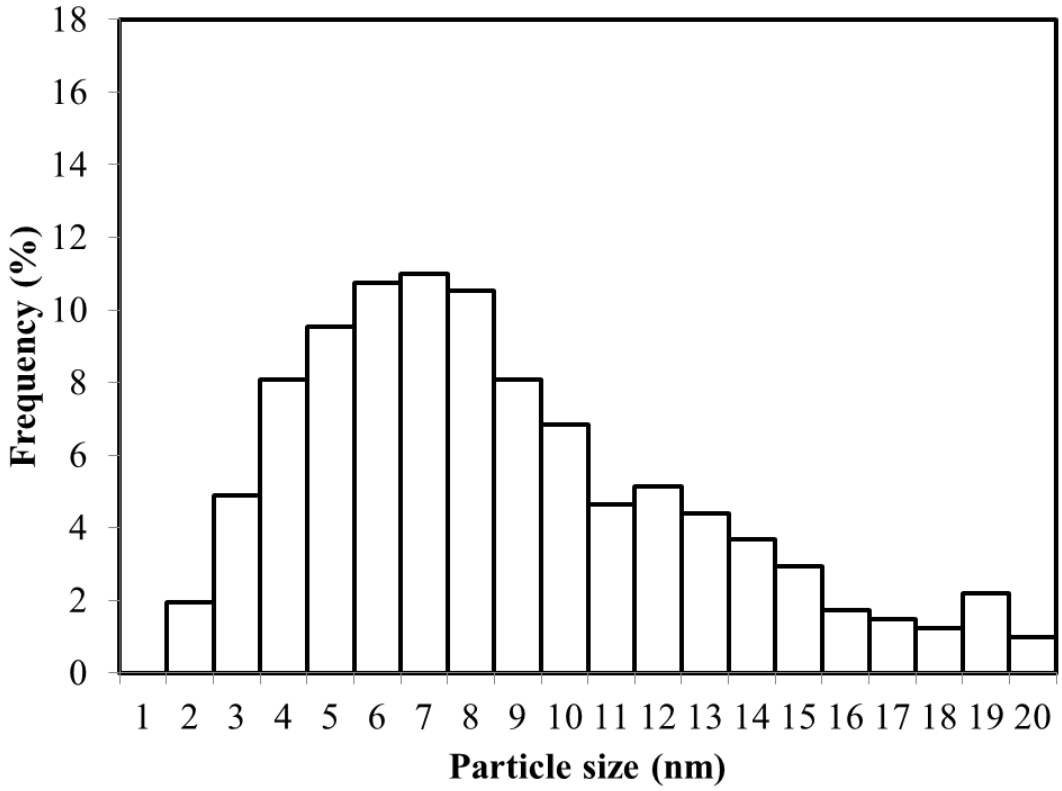
Frequency (%)
0
2
4
6
8
10
12
14
16
18
1 2 3 4 5 6 7 8 9 10 11 12 13 14 15 16 17 18 19 20
Particle size (nm)

Fig. 10a

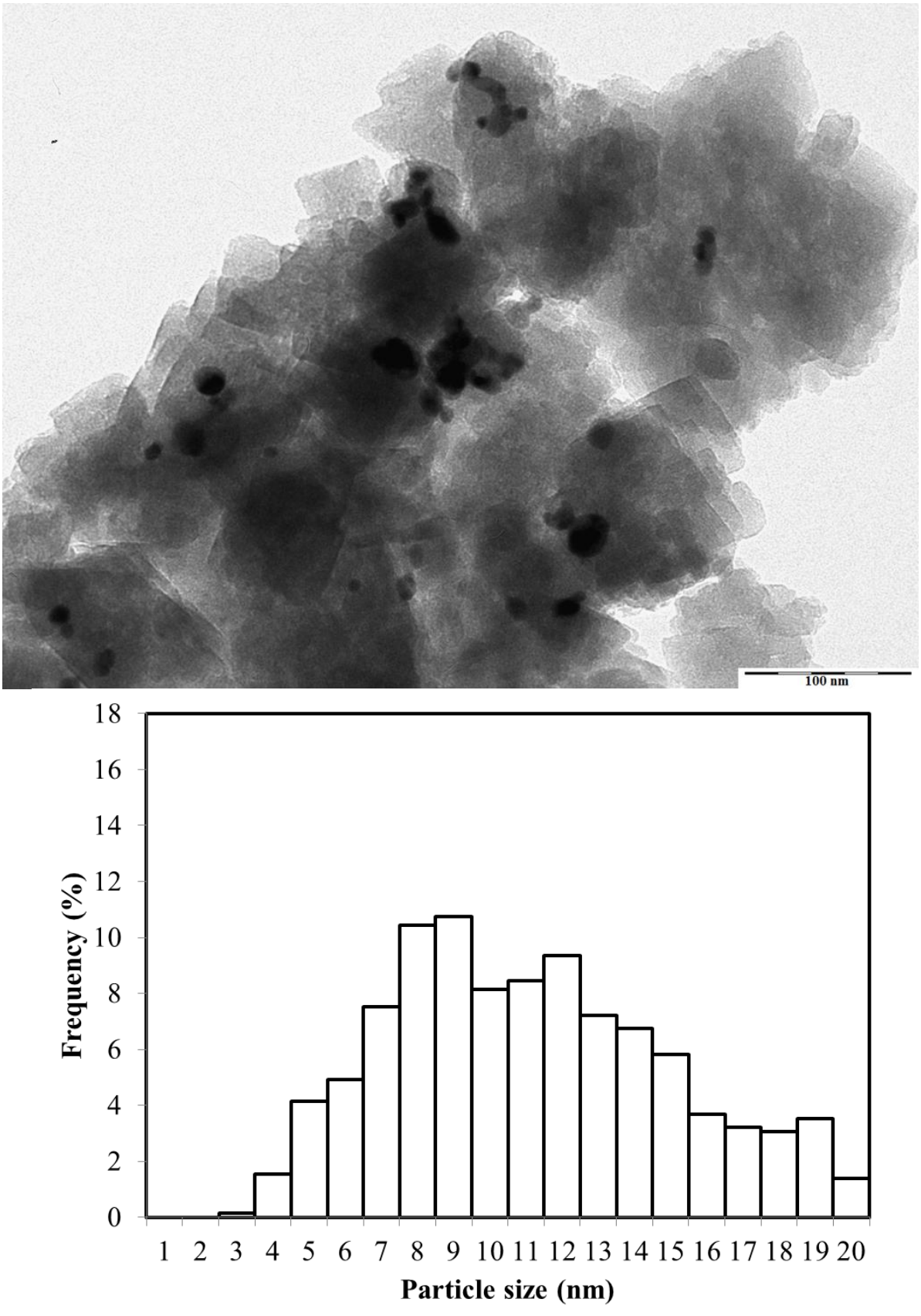
100 nm
Frequency (%)
0
2
4
6
8
10
12
14
16
18
1 2 3 4 5 6 7 8 9 10 11 12 13 14 15 16 17 18 19 20
Particle size (nm)

Fig. 10b